Journal of Renewable Energy and Smart Systems Vol.1 No.1, 2024:64-72

Renewable Energy and Smart Systems

journal homepage: https://sanad.iau.ir/journal/res

A wide range of communication wavelengths; the tunable zero-dispersion by dual-concentric-core photonic crystal fibers

M. R. karimipour[1,3] , A. S. Naeimi[2,3*]

[1]*Department of Electrical Engineering, Aliabad Katoul Branch, Islamic Azad University, Aliabad Katoul, Iran*

[2]*Department of Physics, Aliabad Katoul Branch, Islamic Azad University, Aliabad Katoul, Iran*

[3] *Energy Research Center, Aliabad Katoul Branch, Islamic Azad University, Aliabad Katoul, Iran*

Article info

Keywords:
photonic crystal fibers
dispersion
dual-concentric

Article history:
Received: 27 May 2024
Accepted: 10 Jul 2024

Abstract

In the present paper, we propose a new Photonic Crystal Fiber (PCF) design and analyze the contribution of geometrical parameters to the photonic crystal fibers dispersion and effective refractive index. The proposed design is validated using the 3-D finite-difference time-domain technique. According to the results of this paper, by increasing the radius of the core, the dispersion coefficient sign changes from positive to negative. For a radius of 0.5 μm at wavelengths above 1600 nm, the dispersion is close to zero. For a core refractive index greater than 1.47, the dispersion will be zero. By increasing the core refractive index, the zero-dispersion wavelength is increased.

1. Introduction

The subject of Photonic Crystal Fibers (PCFs) has recently received remarkable attention as a result of their unique specifications in photonic and optic applications [1]. In early literature, PCF was only employed as an optical communication channel [2]. Over time, the researchers have proven that the PCFs can be impressively implemented in a variety of promising applications, such as imaging and sensing [5,6], nonlinear optics [3], biomedical technology [7], high power applications [4], spectrometry [8], laser applications [10], supercontinuum generation [9],

chemical sensing [11], remote sensing applications [12], etc.

In recent years, the detection of various chemical agents using PCF-based sensors has triggered a new research subject for researchers due to their higher precision, sensitivity, and faster response. Based on the core arrangement, PCFs can be classified into three categories: solid core, porous core, and hollow-core PCFs [5]. Of these three types, the porous core and hollow-core PCFs can be implemented for chemical sensing purposes in sensing applications.

Given its intense effect on temporal optical pulse shape, the chromatic dispersion of optical fibers is among the most significant parameters considered in optical communication systems. In order to compensate for the chromatic dispersion of the fibers, different strategies have been adopted, such as Bragg grating fibers [15], electronic dispersion compensation [14], conventional dispersion compensating fibers (DCFs) [13], and optical phase conjugation [16], etc. Among these techniques, DCF is more frequently used due to its low nonlinearity, negative dispersion, and lower losses [17]. In fact, DCF is vital for high-speed and long-path optical propagation on the basis of standard single-mode fibers (SMFs).

The suggested system is a dual-concentric-core fiber system to compensate for the aggregated SMF dispersion for long-path transmissions [18, 19]. Samiul et al. presented an adjusted octagonal photonic crystal fiber featuring a particular core region shape representing a -465.5 ps/ (nm·km) negative dispersion featuring an absolute dispersion fluctuation equal to 10.5 ps/ (nm·km) enveloping a 215 nm flatness [20]. Xuyou et al. developed a pentagonal PCF design exhibiting a birefringence in the order of 1.75×10-2 and 250 nm flatness with a mean negative dispersion of -474 ps/ (nm·km) [21]. Besides, Shubi et al. presented MO-PCF with only a 95 nm flat band with negative dispersion that ranged within -226 to -290 ps/ (nm·km) [22]. Mahmud et al. proposed a square silica photonic crystal fiber with flatness over only 170 nm. This group has proposed a 230 nm flatness by employing lead-silicate PCF. Compared to silica photonic crystal fiber, the cost of lead-silicate PCF fabrication is much higher as a dispersion compensating fiber [23].

A quad-core hexagonal lattice PCF structure has been studied [24]. The propagation characteristics of both studied structures guarantee their capability of mitigating the PMD effect. Simulated PCF structures are of exceptionally high birefringence and very low dispersion. In addition, confining the modes in individual cores reflects the contribution of quad-core PCFs. Both structures showed exceptionally low confinement losses. In addition, the authors reported a high nonlinear coefficient of 310 W-1Km-1. Also, the noticed normalized frequency value guarantees endless single-mode characteristics of PCFs [24].

By the introduction of control parameters into the PCF cross-section, complicatedly designed PCFs featuring flat dispersion and also three zero-dispersion wavelengths (ZDWs) were developed in order to determine the third extreme point of Dw, and then the fiber core was adjusted to the chosen size so that the dynamic range of Dw was tailored compared to Dm. By fixation of the coordinates of the three ZDWs and the variation of various dispersion slopes, a quantitative control technique for the dispersion curve has been developed. One can control the mismatch degree between progressively decreasing chromatic dispersion and SPM via various dispersion slopes of the Photonic Crystal Fibers with the same three zero-dispersion wavelengths affecting the evolution speed of the direct soliton spectral tunneling (DSST). Also, apart from creating a coherent supercontinuum (SC), this DSST prevents the creation of red-shifted dispersion wavelengths, which are able to degrade the coherent supercontinuum. According to the results of the simulation, the flatter is the dispersion flatness degree, the more uniform the distribution of power of the created coherent supercontinuum and the wider the wavelength range will be. The coverage of coherent SC spectrum created in complicatedly designed Photonic Crystal Fibers featuring 0 ± 3.345 ps/ (nm.km) dispersion ranges within 1281-2200 nm with power variation ranging from −14.8 dB to −9.4 dB [25].

A Photonic Crystal Fibers structure featuring a hexagonal lattice with various materials has been simulated. The considered background material is silica. Applying such material is intended to determine the propagation specifications in Photonic Crystal Fibers with the materials featuring nonlinear and linear behaviors. Nonetheless, the motivation for investigating this structure is reporting low dispersion. Here, a very low dispersion has been reported for the structure. Over a wide range of communication wavelengths, the tunable zero-dispersion has been determined, i.e., the entire structure is considered eligible for being used in medical applications, optical communication systems, and other sensing purposes.

2. Modeling the photonic crystal fiber

As we know, PCF has an air hole core of varying structure. In particular, research reports have studied triangular and square lattice shapes. By reviewing the investigations on all the PCF structures, we have attempted to model dual-concentric-core PCF structures in which two types of PCF structures are integrated in the form of a novel paradigm. We have proposed a hexagonal structure with a triangular lattice for the intended goal. The use of hexagonal structures for inner and outer regions ensures optimal dispersion. The great difference in effective refractive index between clad and core regions greatly contributes to the chromatic dispersion. The structural symmetry prohibits the possibility of linear electro-optic phenomena.

The silica wavelength dependency on the refractive index was subjected to the simulation by the Sell-Meier equation. Also, chromatic dispersion is defined as the frequency dependence of the phase velocity of the light wave. Dispersion D in ps/nm/km of a photonic crystal fiber is estimable via calculation of the value of effective refractive index (n_{eff}) with respect to the wavelength by Eq (1):

$$D = -\frac{\lambda}{c}\frac{d^2\,\mathrm{Re}[n_{eff}]}{d\lambda^2} \qquad (1)$$

Here, λ is the wavelength, c denotes the light velocity in vacuum, and [n_{eff}] stands for the real part of the refractive index.

In addition, the fiber dispersion (D) is dependent on geometric specifications, such as the diameter of inner and outer circular holes, pitch, and shape of air holes. By investigating these parameters, appropriate guiding specifications will be determined. As we know, the dispersion is related to the real part of the refractive index, and confinement losses are related to the imaginary part of the refractive index with wavelength. Note that Equation (2) presents the association between group velocity and refractive index.

$$v_g = \left(\frac{\partial\kappa}{\partial\omega}\right)^{-1} = c\left(\frac{\partial}{\partial\omega}\left(\omega n_{eff}\right)^{-1}\right) = \frac{(\quad c}{2\quad n_{eff}) + \omega\frac{\partial n}{\partial\omega}} = \frac{c}{n_g(\omega}$$

where n_g stands for the group index. Also, the wavenumber k is describable as the changes occurred in spectral phase per unit length. Besides, the effective nonlinearity of the fiber can be calculated in the fiber core.

$$\gamma = \frac{2\pi n_2}{\lambda A_{eff}} \qquad (3)$$

The effective nonlinear coefficient is computed using Eq (3). In this equation, n_2 is a nonlinear coefficient of the material, and A_{eff} is the effective modal area.

3. Results and Discussion

This simulation is performed using the FDTD solver with boundary conditions of the perfectly matched layers (PMLs). The FDTD method is known as a efficient and robust tool for modeling the direct numerical analyses of the time-dependent Maxwell equations. This technique provides us with robust and effective analysis and simulation of even submicron devices featuring very fine details in structures. In this paper, dual-concentric-core PCF will be used to achieve less dispersion. In terms of fiber, this fiber is

constituted of a triangular network of air holes featuring an L step (23.2 µm) in the silica substrate (Corning 7980 Silica), which has a core of a radius r=300 µm and a refractive index of n (1.4 for wavelengths of 1.4-1.7 microns). The internal cladding consists of two layers of air holes (diameter of d1=7.73 µm) and the second core, i.e., the third air holes layer featuring a smaller diameter (d2=4.64 µm), and external cladding is constituted of two layers of air holes with diameter d3 (5.8 µm), which is shown in Figure 1. In this figure, the coordinates of 1 to 6 holes are (23.2, 0), (46.4, 0), (69.2, 0), (92.8, 0), (116, 0), and (11.6, 20), respectively.

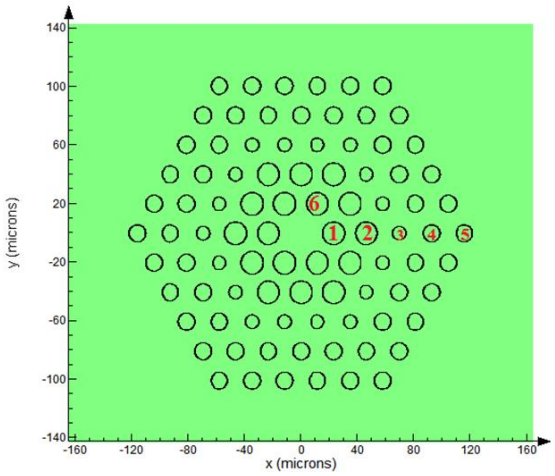

Figure 1. Schematic of Dual-concentric-core PCF

Dual-concentric-core PCFs offer a micro-structured air-hole cladding covering the silica core. The hallow cladding of the micro-structure results in a negative core-cladding difference in refractive index. Thus, the photonic crystal fiber may not operate by total internal reflection (TIR). Nevertheless, a suitably designed holey photonic crystal cladding, running along the whole length of fiber, may avoid light evasion from the fiber core. Using suitable choices for the PCF design parameters, the power coupling between the fundamental multicore fiber mode and the fundamental mode of the PCF may be much higher compared to those between the other super modes and the fundamental mode. Thus, on the right side of the multicore fiber laser cavity, the fundamental multicore fiber mode is of the maximum power reflection coefficient, which dominates the power of the output laser. Given that for the fundamental multicore fiber mode, the maximum power will result in the desired profile of the laser beam, the higher fraction of the fundamental multicore fiber mode power restrained in the entire output power improves the beam quality. Under these circumstances, if a photonic bandgap takes place, light transmission becomes feasible. Fig. 2 shows the simulated fundamental mode located within the bandgap.

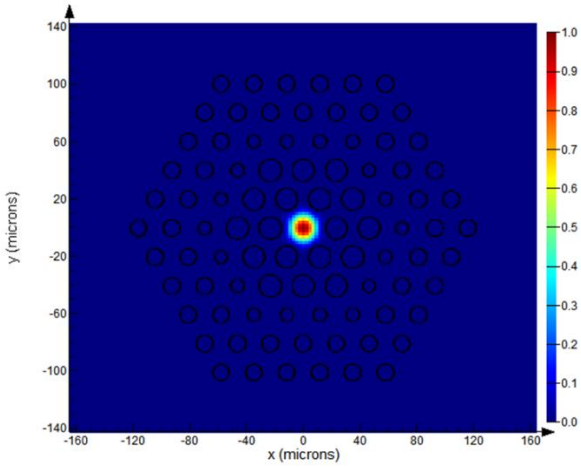

Figure 2. The results of the fundamental mode simulation

In Figure 3, for the refractive indices equal to 1.5, the core radius changes from 0.25 µm to 1 µm. One can design a PCF structure featuring a flat dispersion curve and three ZDWs via modification of structural parameters (the diameter of small air holes embedded between standard lattices within the third and the first rings) and the size of the fiber core in order to acquire the desired shape, the dynamic range of waveguide dispersion (D_w) curve, and the number of extreme points. In order to design another Photonic Crystal Fiber with a slightly larger dispersion slope and the same zero-dispersion wavelengths, a quantitative approach must be suggested, which is realized via fixation of the ZDW positions and adjusting various dispersion slopes. According to this figure, by

increasing the radius of the core, the sign of the dispersion coefficient is changed from positive to negative. For a radius of 0.5 µm at wavelengths above 1600 nm, the dispersion is near zero. As the radius of the core increases, at low wavelengths, the dispersion exhibits strongly nonlinear behavior. According to this figure, with the increase of the passing wavelength, it shows a linear behavior and tends to zero.

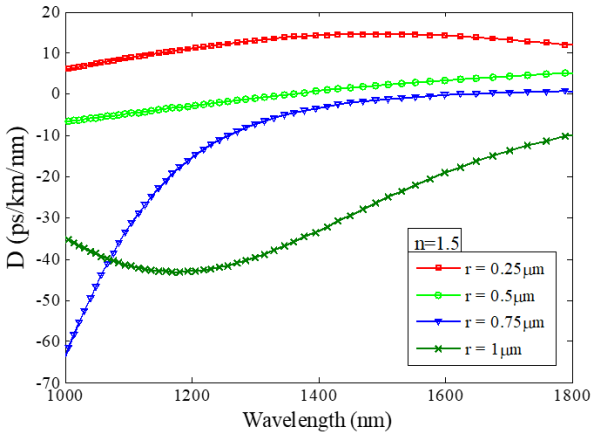

Figure 3. The effect of radius changes on dispersion for n=1.5 and radius of 0.25 µm to 1 µm

In Figure 4, for a refractive index of 1.5, the core radius will be changed from 25.2 µm to 2 µm. A ZDW will split optical spectra into two areas with anomalous and normal dispersion. While pumping the regular area of dispersion of a nonlinear medium, spectral broadening predominantly takes place through self-phase modulation (SPM) that results in a coherent spectrum immediately. At the same time, sequential stimulated Raman scattering (SRS) in the pulse will pass on energy from higher to lower frequencies constantly. In order to acquire a more encompassing coherent spectrum, the entire normal dispersive fibers are employed in order to create supercontinuum spectra. Pumping in the anomalous dispersion area leads to the domination of soliton dynamics, which is primarily consisted of soliton fission (SF), SPM, blue-shifted dispersive waves (DWs), as well as soliton self-frequency shift (SSFS). Also, as a result of phase matching, four-wave mixing (FWM) and cross-phase modulation (XPM) are created on the left side of zero-dispersion wavelength, leading to development of a blue-shift in the trapped wave. The whole spectrum is divided by two zero-dispersion wavelengths into three dispersion areas, namely, two areas featuring normal dispersion sandwich an area of abnormal dispersion. In comparison with Photonic Crystal Fibers featuring zero-dispersion wavelengths, SSFS features a distinct redshift boundary located close to the second zero-dispersion wavelength. When a negative dispersion slope is present close to the second ZDW, it leads to a redshift in DWs in the trapped wave and the second area of normal dispersion as a result of phase matching between the red-shifted DWs and the red-shifted soliton. In fact, the former flattens the SC located between red-shifted DWs and redshift soliton; however, the latter effect extends the SC to the red end. Three zero-dispersion wavelengths split optical spectra into four dispersion areas, and solitons within the first region of anomalous dispersion may tunnel into the second region of anomalous dispersion leading to more expansion of the spectra. In this figure, the dispersion shows linear behavior with increasing the core radius. According to this figure, the dispersion coefficient is negative with increasing the core radius. As soon as the radius of the core increases, the dispersion changes approximately by -29 ps/km/nm.

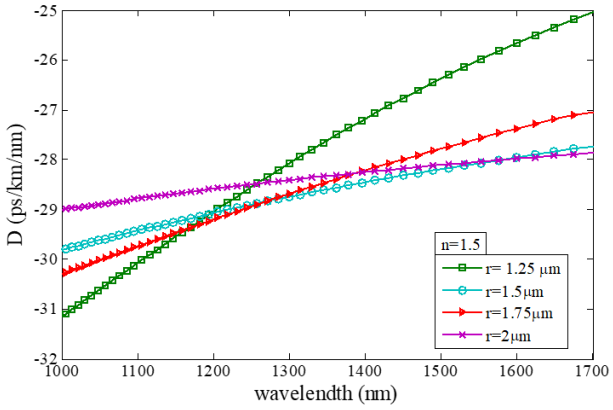

Figure 4. The effect of radius changes on dispersion for n=1.5 and radius of 1.25 µm to 2 µm

The following figure investigates the effect of radius changes on the effective refractive index. In Figure 5, for a refractive index of 1.5, the core radius is changed from 0.25 µm to 2 µm. The effective refractive index

behaves almost linearly with wavelength. As the radius increases, the refractive index increases nonlinearly. By increasing the refractive index radius, we find a nonlinear state and observe fewer changes in it. The refractive index decreases with increasing the wavelength.

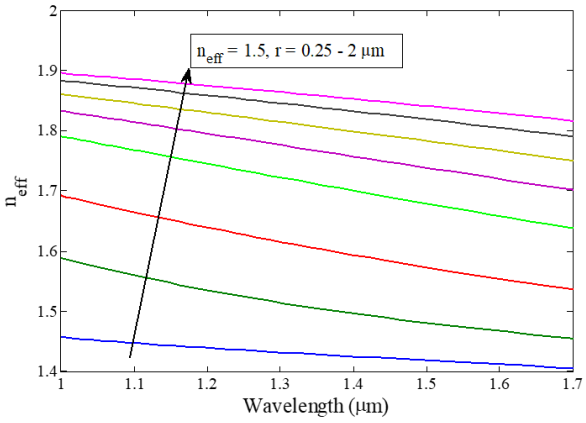

Figure 5. The effect of radius changes on effective refractive index

In Figure 6, for a radius of 1.25, the core refractive index is changed from 1.45 to 1.49. According to this figure, it has a nonlinear behavior at a low refractive index and shows linear behavior with increasing the refractive index. However, for a core refractive index greater than 1.47, the dispersion will be zero. By increasing the core refractive index, the zero-dispersion wavelength is increased. For the refractive index of 1.47, the zero-dispersion wavelength was 1100 nm. Also, for the refractive index of 1.48, the zero-dispersion wavelength was 1300 nm, and for the refractive index of 1.49, the zero-dispersion wavelength was 1500 nm.

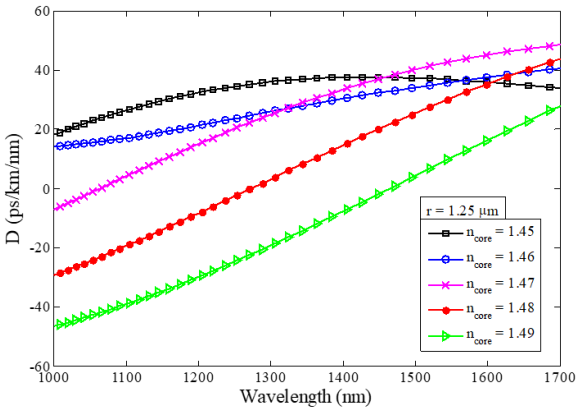

Figure 6. The effect of changes in refractive index on the dispersion

Conclusion

We investigated the impact of geometrical parameters on the PCF dispersion and effective refractive index. This analysis is accomplished by using perfectly matched layers boundary condition in FDTD method. Based on results of this paper, by increasing the radius of the core, the sign of the dispersion coefficient is changed from positive to negative. For a radius of 0.5 µm at wavelengths above 1600 nm, the dispersion is close to zero. For a core refractive index greater than 1.47, the dispersion will be zero. By increasing the core refractive index, the zero- dispersion wavelength is increased.

References:

[1]. Habib A, Anower S, Hasan R (2017) Ultrahigh birefringence and extremely low loss slotted-core microstructure fiber in terahertz regime. Curr Opt Photon 1:567–572.

[2]. Faruk MM, Khan NT, Biswas SK (2019) Highly nonlinear bored core hexagonal photonic crystal fiber (BC-HPCF) with ultra-high negative dispersion for fiber optic transmission system. Front Opto electron.

[3]. Travers JC, Chang W, Nold J, Joly NY (2011) PJ Russell (2011)‘‘Ultrafast nonlinear optics in gas-filled

hollow-core photonic crystal fibers [Invited]''. J Opt Soc Am B 28:A11–A26

[4]. Robin C, Dajani I, Zeringue C, Ward B, Lanari A (2012) Gain-tailored SBS suppressing photonic crystal fibers for high power applications. Proc SPIE Fiber Syst Appl 1:82371D.

[5]. Habib MA (2020) A Refractive index based micro-structured sensorfor blood components detection in terahertz regime. SensorLetters 18(1):74–82

[6]. Lobo Ribeiro AB, Silva SFO, Fraza˜o O, Santos JL (2019) Bi-coreoptical fiber for sensing of temperature, strain and torsion.Measure Sci Technol 30:035104

[7]. Vaiano P, Carotenuto B, Pisco M, Ricciardi A, Quero G, Consales M,Crescitelli A, Esposito E, Cusano A (2016) Lab on fibertechnology for biological sensing applications. Laser PhotonicsRev 10(6):922–961.

[8]. Knabe K, Shun Wu, Lim J, Tillman KA, Light PS, Couny F, WheelerN, Thapa R, Jones AM, Nicholson JW, Washburn BR, BenabidF, Corwin KL (2009) 10 kHz accuracy of an optical frequencyreference based on12C2H2-filled large-core kagome photonic crystal fibers. Opt Express 17:16017–16026

[9]. Wadsworth WJ, Ortigosa-Blanch A, Knight JC, Birks TA, Martin Man T-P, Phillip St J (2002) Super continuum generation in photonic crystal fibers and optical fiber tapers: a novel light source. J Opt Soc Am B 19:2148–2155

[10]. Humbert G, Knight JC, Bouwmans G, Russell PJ, Williams DP,Roberts PJ, Mangan BJ (2004) Hollow core photonic crystal fibers for beam delivery. Opt Express 12:1477–1484

[11]. Islam MR, Kabir MF, Talha KMA, Islam MS (2019) A novel hollowcore terahertz refractometric sensor. Sens Biosens Res 5:100295.

[12]. Liu C, Weiquan Su, Liu Q, Xili Lu, Wang F, Sun T, Chu PK (2018) Symmetrical dual D-shape photonic crystal fibers for surfaceplasmon resonance sensing. Opt Express 26:9039–9049.

[13]. B. Zsigri, J. Lægsgaard, and A. Bjarklev, "A novel photonic crystal fibre design for dispersion compensation," J. Opt. A Pure Appl. Opt., vol. 6, no. 7, pp. 717–720, Jul. 2004.

[14]. N. M. Litchinitser, B. J. Eggleton, and D. B. Patterson, "Fiber Bragg gratings for dispersion compensation in transmission: Theoretical model and design criteria for nearly ideal pulse recompression," J. Light. Technol., vol. 15, no. 8, pp. 1303–1313, 1997.

[15]. H. Bülow, F. Buchali, and A. Klekamp, "Electronic dispersion compensation," J. Light. Technol., vol. 26, no. 1, pp. 158–167, 2008.

[16]. S. Watanabe, T. Naito, and T. Chikama, "Compensation of chromatic dispersion in a single-mode fiber by\noptical phase conjugation," IEEE Photonics Technol. Lett., vol. 5, no. 1, pp. 92–95, Jan. 1993.

[17]. A. Bala, K. R. Chowdhury, M. B. Mia, and M. Faisal, "Highly birefringent, highly negative dispersion compensating photonic crystal fiber," Appl. Opt., vol. 56, no. 25, p. 7256, Sep. 2017.

[18]. K. Thyagarajan, R.K. Varshney, P. Palai, A.K. Ghatak, and I.C. Goyal, "A novel design of a dispersion compensating fiber," IEEE Photonics Technol. Lett. 8, 1510-1512 (1996).

[19]. J.-L. Auguste, R. Jindal, J.-M. Blondy, M. Clapeau, J. Marcou, B. Dussardier, G. Monnom, D.B. Ostrowsky, B.P. Pal, and K. Thyagarajan, "−1800 ps/(nm·km) chromatic dispersion of 1.55 μm in dual concentric core fibre," Electron. Lett. 36, 1689-1691 (2000).

[20]. HABIB, M. S., AHMAD, R., HABIB, M. S. et al. Residual dispersion compensation over the S +C +L +U wavelength bands using highly birefringent octagonal photonic crystal fiber. Applied Optics, 2014, vol. 53, no. 14, p. 3057–3062.

[21]. LI, X., LIU, P., XU, Z., et al. Design of a pentagonal photonic crystal fiber with high

birefringence and large flattened negative dispersion. Applied Optics, 2015, vol. 54, no. 24, p. 7350–7357.

[22]. KAIJAGE, S. F., NAMIHIRA, Y., HAI, N. H., et al. Broadband dispersion compensating octagonal photonic crystal fiber for optical communication applications. Japanese Journal of Applied Physics, 2009, vol. 48, no. 052401, 8 p.

[23]. MAHMUD, R. R., KHAN, M. A. G., RAZZAK, S. M. A. Design and comparison of SF57 over SiO2 on same structured PCF for residual dispersion compensation. Photonics Journal, 2016, vol. 8, no. 6, 10 p. DOI: 10.1109/JPHOT.2016.2628802.

[24]. Kumar, P., Kumar, V. and Roy, J.S., 2019. Design of quad-core photonic crystal fibers with flattened zero dispersion. *AEU-International Journal of Electronics and Communications*, *98*, pp.265-272.

[25]. Huang, Y., Yang, H., Zhao, S., Mao, Y., & Chen, S. (2021). Design of photonic crystal fibers with flat dispersion and three zero dispersion wavelengths for coherent supercontinuum generation in both normal and anomalous regions. *Results in Physics*, *23*, 104033.